Scripta Materialia 204 (2021) 114122

Contents lists available at ScienceDirect

Scripta Materialia

journal homepage: www.elsevier.com/locate/scriptamat

Hydrogen-induced transgranular to intergranular fracture transition in bi-crystalline nickel

Yu Ding[a], Haiyang Yu[b], Kai Zhao[c], Meichao Lin[a], Senbo Xiao[a], Michael Ortiz[d], Jianying He[a], Zhiliang Zhang[a,*]

[a] Department of Structural Engineering, Norwegian University of Science and Technology (NTNU), Trondheim 7491, Norway
[b] Division of Applied Mechanics, Department of Materials Science and Engineering, Uppsala University, Uppsala SE-75121, Sweden
[c] Jiangsu Key Laboratory of Advanced Food Manufacturing Equipment and Technology, Jiangnan University, Wuxi 214122, China
[d] Graduate Aerospace Laboratories, California Institute of Technology, 1200 E. California Blvd., Pasadena, CA 91125, United States

ARTICLE INFO

Article history:
Received 31 May 2021
Revised 28 June 2021
Accepted 28 June 2021

Keywords:
Hydrogen embrittlement
Fracture
Grain boundary
Molecular dynamics (MD)

ABSTRACT

It is known that hydrogen can influence the dislocation plasticity and fracture mode transition of metallic materials, however, the nanoscale interaction mechanism between hydrogen and grain boundary largely remains illusive. By uniaxial straining of bi-crystalline Ni with a Σ5(210)[001] grain boundary, a transgranular to intergranular fracture transition facilitated by hydrogen is elucidated by atomistic modeling, and a specific hydrogen-controlled plasticity mechanism is revealed. Hydrogen is found to form a local atmosphere in the vicinity of grain boundary, which induces a local stress concentration and inhibits the subsequent stress relaxation at the grain boundary during deformation. It is this local stress concentration that promotes earlier dislocation emission, twinning evolution, and generation of more vacancies that facilitate nanovoiding. The nucleation and growth of nanovoids finally leads to intergranular fracture at the grain boundary, in contrast to the transgranular fracture of hydrogen-free sample.

As indicated by its name, a key feature of hydrogen embrittlement (HE) [1–3] is the transition from ductile to "brittle" fracture in the presence of hydrogen. For polycrystalline materials, this transition is usually attributed to hydrogen-induced transgranular to intergranular fracture at the microscopic scale, observed in a large number of *ex-situ* experiments [4–7]. All the studies [8–16] show that grain boundary (GB) plays an important role in HE and the hydrogen-GB interactions hold the key to understanding the transgranular to intergranular fracture transition. Nowadays, it is well understood that the transition process may involve the synergistic action of several important HE mechanisms [11,17]. Three widely accepted mechanisms are hydrogen enhanced local plasticity (HELP), hydrogen enhanced decohesion (HEDE), and hydrogen enhanced strain-induced vacancy formation (HESIV). The theory of HELP [18–22] is based on the experimental evidence of enhanced dislocation mobility and well-evolved dislocation structures beneath the fracture surfaces of hydrogen-embrittled samples. However, there is still a large gap in the understanding of how this locally ductile behavior could lead to the eventual "brittle" fracture. HEDE [23–27] postulates that local accumulation of H at crack tips could contribute to the weakening of metal bonds resulting in fracture, but it does not make an explanation for the enhanced plasticity. HESIV [28–32] assumes that the vacancy clusters generated during plastic deformation are stabilized by forming H-vacancy complexes, which will further interact with the dislocations. However, the connection of those stabilized vacancies to embrittlement remains unexplained. All these mechanisms can be viable at the GBs, which is a material interface with intensive dislocation activity and high *H* trapping capacity [33]. The hydrogen-enhanced plasticity mediated failure mechanism [3] has been proposed as a connection between HELP and HEDE, trying to make a universal explanation to HE phenomena. It should be mentioned that the whole framework was established as a posteriori interpretation of evolved microstructures. The transition process of the fracture mode has not been directly demonstrated by *in-situ* experiment or simulation. Verification of this mechanism is one of the outstanding issues in HE research.

The interaction between hydrogen and grain boundary/material interface has been simulated both using the continuum approach [34] and the atomistic method [35]. Hydrogen segregation around GBs [36,37] and the influence of hydrogen on the propagation of an existing crack [38] have been elaborated. However, the direct transgranular to intergranular transition without an initial crack

* Corresponding author.
E-mail address: zhiliang.zhang@ntnu.no (Z. Zhang).

https://doi.org/10.1016/j.scriptamat.2021.114122

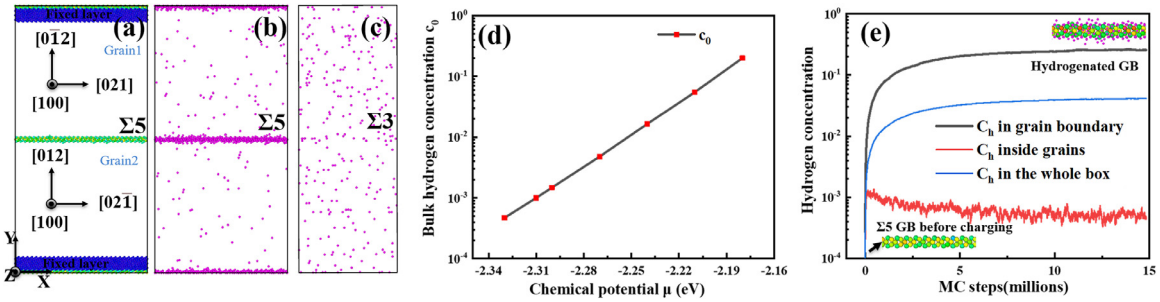

Fig. 1. (a) Equilibrium structures of perfect Σ5(210)[001] GB. (b, c) *H* distribution map for Σ5 GB and Σ3 CTB, respectively. (d) The relationship between Equilibrium bulk *H* concentration c_0 in perfect FCC Ni and chemical potential μ used in the charging process. (e) *H* concentration in the GB region (1 nm around GB), inside the grains, and in the whole box as a function of MC charging time.

has not been observed. Recent experimental studies [39–41] indicate that mobile H-deformation interaction is not an intrinsic requirement for H-induced intergranular fracture, implying that the initial *H* segregation on the GB is the key. But it is still unclear how the segregated *H* interacts with the GB. The present work zooms into the GB region with segregated *H* and probes the mechanisms behind H-induced intergranular fracture. A Σ5(210)[001] GB was created by constructing two separate crystals with desired crystallographic orientations and joining them along a plane normal to the Y-direction (Fig. 1a). The initial configuration was then modified by shifting the upper grain in the X-Z plane, deleting overlapping atoms, and applying the conjugate gradient method to equilibrate the system. The simulation box was divided into three regions: The vicinity ±1 nm to the GB as GB region, 1 nm thick region on the top of grain1 and bottom of grain2 as boundary layers to apply displacement controlled loading, and rest part as grains. Periodic boundary conditions were imposed along the *X* and *Z* directions while a free boundary condition was employed along the *Y* direction. After equilibrium in the isothermal–isobaric (NPT) ensemble at 300 K for 100 ps, the mixed grand canonical Monte Carlo (GCMC)/molecular dynamic (MD) method was utilized to obtain the dynamic trapping map around the GB. For the GCMC implementation, the system was kept at constant chemical potential μ, volume *V* and temperature *T*. There is a relationship between chemical potential μ and equilibrium bulk *H* concentration c_0 in perfect lattice: $\mu = kT \ln c_0 + \Delta E$, where ΔE is the segregation energy of one *H* atom and *k* is the Boltzmann constant. During the *H* charging process, each step of GCMC runs (insertion or deletion of one randomly chosen *H* atom) was followed by 50 steps of MD runs in canonical (NVT) ensemble until the *H* concentration fluctuates in a narrow range (±1% atomic ratio). The simulations were first performed for the perfect FCC Ni lattice without GB, to obtain the relationship between c_0 and μ (Fig. 1d). Then $\mu = -2.31$ eV was chosen as the charging parameters for all the subsequent study corresponding to $c_0 = 0.001$ in the bulk grain. The equilibrium hydrogenated GB after charging was regarded as the 100% saturation case with the 0, 13, 25, 40, 60% saturation cases as comparison. After charging, the system was relaxed in the NPT ensemble for 100 ps. To obtain a realistic stress state in front of a crack tip and avoid unphysical elongation, uniaxial straining in the NVT ensemble was carried out by moving the upper boundary layer at a constant velocity of 2 m/s along *Y* direction while the lower layer is kept stationary. The atomic stress during deformation was analyzed by Viral theory [42], illustrations of all simulation snapshots were achieved by the coordination number centrosymmetry parameter [43] and common neighbor analysis (CNA) [44], and dislocations were identified by Ovito [45].

The *H* distribution during charging is shown in Fig. 1e. The *H* concentration in the grains and GB reaches $c_0 = 0.001$ in the first 100,000 MC steps. *H* atoms continue to pump into the GB region due to the high trapping energy and excess volumes in the subsequent MC steps. However, the *H* concentration inside the grains is slightly reduced and kept around $c = 0.0008$, which is mainly caused by the attractive interaction between the formed *H* atmosphere around the GB and newly inserted H. Finally, the GB structure reaches an equilibrium at $c = 0.25$ after 15,000,000 MC steps in Fig. 1b. The locally high *H* concentration agrees well with the experimental results [33] and theoretical calculation [46], indicating that this type of Σ5 GB could be a preferred gathering site for H. For comparison, a Σ3 coherent twin boundary (CTB) is charged under the same conditions. The evenly distributed *H* in Fig. 1c implies that CTB has an inconsequential effect to trap *H* because of the compact structure and few trapping sites, indicating that CTBs have good resistance to HE [16,47].

Fig. 2a shows the stress (Syy)-strain curve in the *Y* direction with varying *H* concentrations during deformation. Fig. 2c–h are the snapshots of the elastic stage, plastic stage, and final fracture for the cases without *H* and with *H* in the 100% saturation case, respectively. Without *H*, the sample fractured ($\varepsilon = 0.208$) with nanovoid nucleation in the grains near the upper boundary layer due to the accumulation of high-density dislocations. With *H* in the 100% saturation case, the sample fractured ($\varepsilon = 0.173$) with nanovoid nucleation on the GB. This shift of nanovoid nucleation site from grain interior to the GB caused by *H* is manifested as H-induced transgranular to intergranular fracture transition. The sample deforms mainly through the nucleation and gliding of 1/6<112> Shockley dislocations (green pipelines) and leaves the twins (red stacking fault) on the path in which they have glided. At the first drop of stress (critical stress), the twins start to grow and soon get pinned by the top and bottom boundary. The inserted *H* could facilitate earlier twinning nucleation ($\varepsilon = 0.08$ without *H* and $\varepsilon = 0.062$ with H) and decrease the critical stress (Syy = 11.06 GPa without *H* and $\varepsilon = 9.55$ GPa with *H*) during this stage. Higher *H* concentration could amplify those effects. To release the stress caused by subsequent deformation, more dislocations nucleate, multiplicate and exit on the GB, which generates more twins. These twins interact with each other in the junctions, further increasing the dislocation density. As shown in Fig. 2b, the twins volume fraction evolution displays a zig-zag pattern until fracture, which is the main plasticity activity during deformation. It should be noted that hydrogen promoted deformation twinning, revealed in the MD simulation, has not been experimentally observed in typical Ni microstructures [39,48–50]. This is probably because the MD simulation assumes no pre-existing dislocations before deformation, so continued plasticity dominated by dislocation gliding was source-controlled and twinning was facilitated, this can be the case for nanocrystalline Ni [51,52]. Therefore, caution should be taken when applying hydrogen-induced twinning mechanism in Ni, since this is likely applicable to highly specialized cases instead of the typical coarse-grained microstructures.

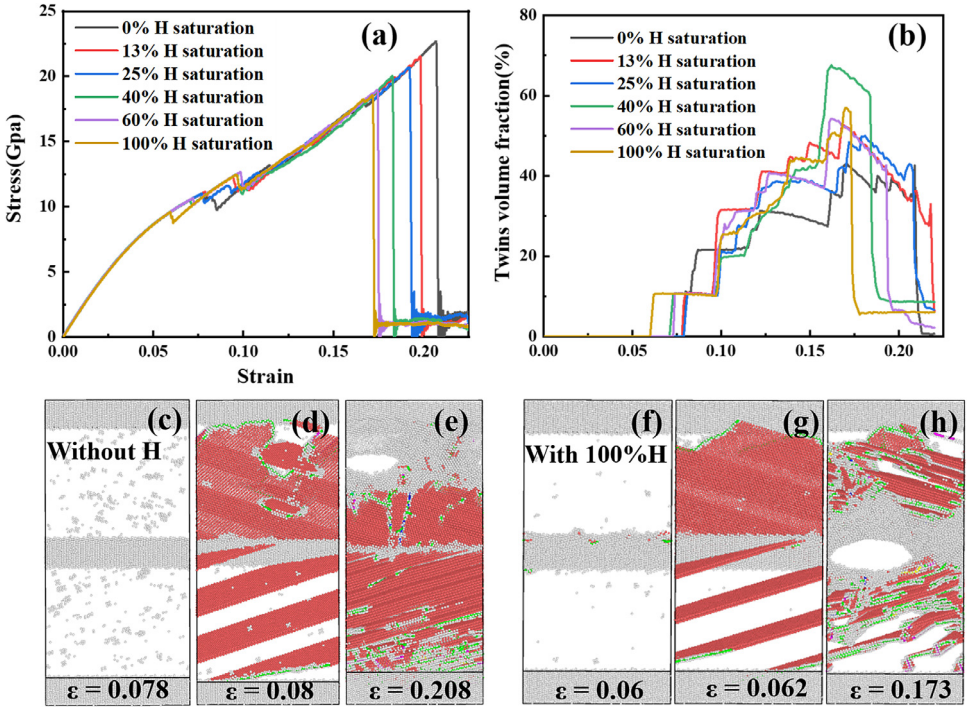

Fig. 2. (a) stress-strain curve in the *Y* direction for varying *H* concentrations. (b) Twins volume fraction as a function of strain with varying *H* concentration. (c–e) atomic structure without H at different strains. (f–h) atomic structure with 100% *H* at different strains. Only atoms in defect structure are colored, HCP atoms are marked red, white atoms indicate other type atoms, and green pipelines outline the 1/6<112> Shockley dislocations.

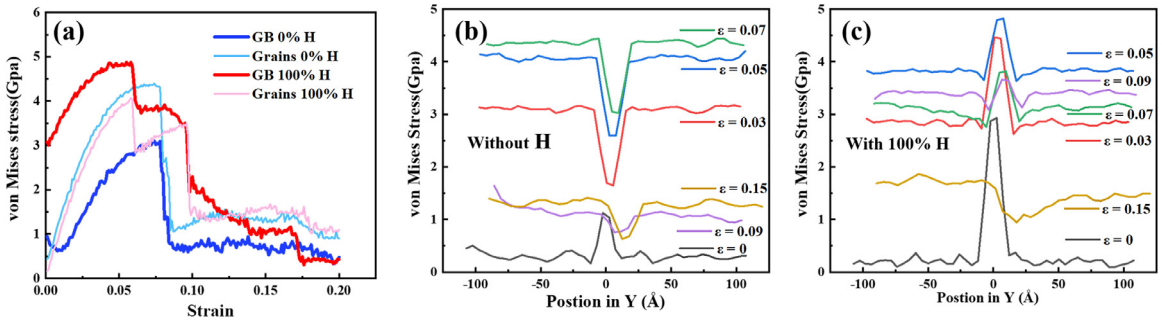

Fig. 3. (a) Average Von Mises stress-strain curve in different regions. (b, c) Average Von Mises stress distribution along the *Y* direction without or with *H*, respectively.

Nevertheless, this can still be a viable mechanism in a number of FCC alloys that undergo deformation twinning, such as in TWIP steels [53,54] or those with nanocrystalline grain structures. To better understand how *H* influences local plasticity, the average von Mises stress distribution along the *Y* direction in different regions is plotted in Fig. 3. It is interesting to note that in Fig. 3b the Σ5(210)[001] GB could release the initial stress and always keep its stress level lower than in the grains during deformation without H. This might be a good explanation for the huge amount of point defects in the grains without *H* (Fig. 2c) and the eventual transgranular fracture. The saturated *H* can increase the initial stress concentration in the GB region and more importantly inhibit the stress-releasing ability of the GB during deformation. The GB thus stays at an activated state [11] with a more disordered atomistic structure due to the higher stress level maintained at the GB than the grain interior, which induces the earlier twinning nucleation and void formation on the GB. Increased *H* concentration could increase the local stress concentration which induces more serious plastic deformation and earlier fracture.

Another important feature revealed in Fig. 2e,h is nanovoiding. In order to investigate the nanovoid formation mechanism, the process of vacancy formation, which could be the embryo of the final void [31], is analyzed in the GB region. The extremely distorted atoms are identified as vacancy cluster and the vacancy volume fraction-strain curve is plotted in Fig. 4a. It is found that there are few vacancies formed around the GB before twinning nucleation without *H*, but the fraction of vacancy volume comes to grow after more plasticity occurs around the GB. With *H*, the vacancy volume fraction comes to grow in the elastic stage which shows that the GB has entered a plasticity-activated state [33], and the vacancy volume fraction rises with increasing pre-charged *H* concentration. It indicates that *H* accelerates vacancy formation at early plasticity stage on the GB, possibly through lattice dislocation interaction and jog formation. Previous studies also show that vacancies could be stabilized by forming Va-H complexes [31,32], consistent with the high vacancy volume fraction observed in the *H* charged cases. Those Va-H complexes could be the reason for the earlier void formation with *H* in Fig. 4g.

In summary, by scrutinizing the tensile responses of Ni Σ5(210)[001] GB with varied hydrogen concentration using atomistic modeling, we demonstrate a transgranular to intergranular-fracture transition mechanism controlled by hydrogen-influenced

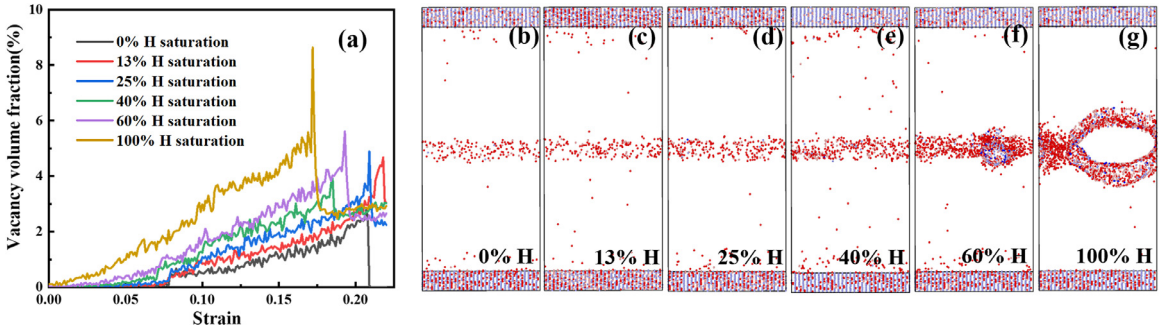

Fig. 4. (a) Vacancy volume fraction as a function of strain with varying H concentration. (b,–g) Snapshots of vacancy surface atoms at strain = 0.18 with varying *H* concentration. Only highly distorted atoms with coordination numbers less than 8 are colored.

plasticity. Compared with the Σ3 coherent twin GB which traps nearly no *H* atoms, *H* will form an atmosphere at the Σ5 GB due to the high trapping energy and excess volume and induce a higher initial local stress. In the case without *H*, less stress is built up at the Σ5 GB region during deformation, which leads to transgranular fracture. In contrast, *H* suppresses the stress-releasing ability of the Σ5 GB, which causes a local stress concentration and promotes local plasticity on the GB. This further leads to early dislocation emission, severe twinning evolution, increased number of vacancies and thus enhanced nanovoiding on the GB. The growth of nanovoids with *H* finally completes the transgranular to intergranular-fracture transition. This work reveals that hydrogen-grain boundary interaction and hydrogen enhanced vacancy formation are important factors in the hydrogen-induced intergranular fracture at room temperature. However, the influence of hydrogen on atomic bonds, i.e. the HEDE mechanism, was not examined here. According to Harris et al. [39], HEDE may play an important part in the process. Therefore, the transgranular to intergranular-fracture transition with hydrogen is likely due to the synergistic action of all the three mechanisms.

Declaration of Competing Interest

The authors declare that they have no known competing financial interests or personal relationships that could have appeared to influence the work reported in this paper.

Acknowledgments

Y.D. acknowledge the financial support provided by the Research Council of Norway under the M-HEAT project (Grant No. 294689). All simulations are carried out on the Fram (Grant No. NN9110K, NN9391K) high-performance computer clusters at NTNU, Trondheim, and Stallo at UiT, Tromsø.

Supplementary materials

Supplementary material associated with this article can be found, in the online version, at doi:10.1016/j.scriptamat.2021.114122.

References

[1] W.H. Johnson, W. Thomson, Proceedings of the Royal Society of London 23 (156-163) (1875) 168–179.
[2] R.P. Gangloff, B.P. Somerday, Gaseous Hydrogen Embrittlement of Materials in Energy Technologies: Mechanisms, Modelling and Future Developments, Elsevier, 2012.
[3] I.M. Robertson, P. Sofronis, A. Nagao, M.L. Martin, S. Wang, D.W. Gross, K.E. Nygren, Metall. Mater. Trans. B 46 (3) (2015) 1085–1103.
[4] S.P. Lynch, J. Mater. Sci. 21 (2) (1986) 692–704.
[5] C.J. McMahon, Eng. Fract. Mech. 68 (6) (2001) 773–788.
[6] M.L. Martin, B.P. Somerday, R.O. Ritchie, P. Sofronis, I.M. Robertson, Acta Mater. 60 (6–7) (2012) 2739–2745.
[7] S. Wang, M.L. Martin, P. Sofronis, S. Ohnuki, N. Hashimoto, I.M. Robertson, Acta Mater. 69 (2014) 275–282.
[8] A. Oudriss, J. Creus, J. Bouhattate, E. Conforto, C. Berziou, C. Savall, X. Feaugas, Acta Mater. 60 (19) (2012) 6814–6828.
[9] J. Chen, A.M. Dongare, J. Mater. Sci. 52 (1) (2017) 30–45.
[10] X. Zhou, D. Marchand, D.L. McDowell, T. Zhu, J. Song, Phys. Rev. Lett. 116 (7) (2016) 075–502.
[11] L. Wan, W.T. Geng, A. Ishii, J.P. Du, Q.S. Mei, N. Ishikawa, H. Kimizuka, S. Ogata, Int. J. Plast. 112 (2019) 206–219.
[12] J.Q. Li, C. Lu, L.Q. Pei, C. Zhang, R. Wang, K. Tieu, Comput. Mater. Sci. 165 (2019) 40–50.
[13] K. Zhao, J.Y. He, Z.L. Zhang, J. Appl. Phys. 127 (1) (2020) 015–101.
[14] H.Y. Yu, J.S. Olsen, V. Olden, A. Alvaro, J.Y. He, Z.L. Zhang, Eng. Fail. Anal. 81 (2017) 79–93.
[15] P. Sestak, M. Cerny, Z.L. Zhang, J. Pokluda, Crystals 10 (7) (2020) 590.
[16] S. Bechtle, M. Kumar, B.P. Somerday, M.E. Launey, R.O. Ritchie, Acta Mater. 57 (14) (2009) 4148–4157.
[17] P. Gong, J. Nutter, P.E.J. Rivera-Diaz-Del-Castillo, W.M. Rainforth, Sci. Adv. 6 (46) (2020) eabb6152.
[18] C.D. Beachem, Metall. Trans. 3 (2) (1972) 437-+.
[19] H.K. Birnbaum, P. Sofronis, Mater. Sci. Eng. A 176 (1–2) (1994) 191–202.
[20] M.L. Martin, J.A. Fenske, G.S. Liu, P. Sofronis, I.M. Robertson, Acta Mater. 59 (4) (2011) 1601–1606.
[21] T. Neeraj, R. Srinivasan, J. Li, Acta Mater. 60 (13–14) (2012) 5160–5171.
[22] A. Nagao, C.D. Smith, M. Dadfarnia, P. Sofronis, I.M. Robertson, Acta Mater. 60 (13–14) (2012) 5182–5189.
[23] A.R. Troiano, Metallogr. Microstruct. 5(6) (2016) 557–569.
[24] J.R. Rice, J.S. Wang, Mater. Sci. Eng. A Struct. 107 (1989) 23–40.
[25] S. Serebrinsky, E.A. Carter, M. Ortiz, J. Mech. Phys. Solids 52 (10) (2004) 2403–2430.
[26] J. Song, W.A. Curtin, Nat. Mater. 12 (2) (2013) 145–151.
[27] A. Tehranchi, W.A. Curtin, Model. Simul. Mater. Sci. 25 (7) (2017).
[28] M. Nagumo, M. Nakamura, K. Takai, Metallurgical and Materials Transactions A 32 (2) (2001) 339–347.
[29] K. Takai, H. Shoda, H. Suzuki, M. Nagumo, Acta Mater. 56 (18) (2008) 5158–5167.
[30] W.A. Counts, C. Wolverton, R. Gibala, Acta Mater. 58 (14) (2010) 4730–4741.
[31] S.Z. Li, Y.G. Li, Y.C. Lo, T. Neeraj, R. Srinivasan, X.D. Ding, J. Sun, L. Qi, P. Gumbsch, J. Li, Int. J. Plast. 74 (2015) 175–191.
[32] Y.X. Zhu, Z.H. Li, M.S. Huang, H.D. Fan, Int. J. Plast. 92 (2017) 31–44.
[33] Y.S. Chen, H.Z. Lu, J.T. Liang, A. Rosenthal, H.W. Liu, G. Sneddon, I. McCarroll, Z.Z. Zhao, W. Li, A.M. Guo, J.M. Cairney, Science 367 (6474) (2020) 171-+.
[34] S. Jothi, T.N. Croft, S.G.R. Brown, Int. J. Hydrog. Energy 39 (35) (2014) 20671–20688.
[35] A. Tehranchi, W.A. Curtin, Eng. Fract. Mech. (216) (2019) 106-502.
[36] C.J. O'Brien, S.M. Foiles, Philos. Mag. 96 (14) (2016) 1463–1484.
[37] C.J. O'Brien, S.M. Foiles, Philos. Mag. 96 (26) (2016) 2808–2828.
[38] A. Tehranchi, W.A. Curtin, J. Mech. Phys. Solids 101 (2017) 150–165.
[39] Z.D. Harris, S.K. Lawrence, D.L. Medlin, G. Guetard, J.T. Burns, B.P. Somerday, Acta Mater. 158 (2018) 180–192.
[40] K. Wada, J. Yamabe, Y. Ogawa, O. Takakuwa, T. Iijima, H. Matsunaga, Mater. Sci. Eng. A Struct. A 766 (2019) 138–349.
[41] S.K. Lawrence, Y. Yagodzinskyy, H. Hanninen, E. Korhonen, F. Tuomisto, Z.D. Harris, B.P. Somerday, Acta Mater. 128 (2017) 218–226.
[42] A.P. Thompson, S.J. Plimpton, W. Mattson, J. Chem. Phys. 131 (15) (2009) 154-107.
[43] C.L. Kelchner, S.J. Plimpton, J.C. Hamilton, Phys. Rev. B 58 (17) (1998) 11085–11088.
[44] J. Schiotz, F.D. Di Tolla, K.W. Jacobsen, Nature 391 (6667) (1998) 561–563.
[45] A. Stukowski, Model. Simul. Mater. Sci. 18 (1) (2010) 015012.
[46] D. Di Stefano, M. Mrovec, C. Elsasser, Acta Mater. 98 (2015) 306–312.
[47] J.Q. Li, C. Lu, L.Q. Pei, C. Zhang, K. Tieu, Scr. Mater. 173 (2019) 115–119.

[48] K.M. Bertsch, S. Wang, A. Nagao, I.M. Robertson, Mater. Sci. Eng. A Struct. 760 (2019) 58–67.
[49] Y. Ogawa, O. Takakuwa, S. Okazaki, K. Okita, Y. Funakoshi, H. Matsunaga, S. Matsuoka, Corros. Sci. 161 (2019) 108–186.
[50] Z.D. Harris, A.W. Thompson, J.T. Burns, Jom-Us 72 (5) (2020) 1993–2002.
[51] X. Wu, Y.T. Zhu, M.W. Chen, E. Ma, Scr. Mater. 54(9) (2006) 1685–1690.
[52] X.L. Wu, E. Ma, Appl. Phys. Lett. 88 (6) (2006).
[53] X. Guo, S. Zaefferer, F. Archie, W. Bleck, Int. J. Miner. Metall. Mater. 28 (5) (2021) 835–846.
[54] C. Zhang, H.H. Zhi, S. Antonov, L. Chen, Y.J. Su, Scr. Mater. 190 (2021) 108–112.